(Received 17 April 2024, Accepted 31 May 2024, Scheduled 17 June 2024)

A Broadband Circularly Polarized Crossed-Dipole Antenna with Wide Axial-Ratio and Gain Beamwidths

Wen Huang, Rui Deng*, and Zhongjie Zhan

School of Optoelectronic Engineering, Chongqing University of Posts and Telecommunications, Chongqing 400065, China

ABSTRACT: A broadband circularly polarized (CP) antenna with both a wide half-power beamwidth (HPBW) and a wide axial ratio beamwidth (ARBW) is proposed. The proposed antenna is composed of a pair of crossed dipoles and a U-shaped metal reflecting cavity. The fan-shaped patches of the dipoles can effectively increase the operating bandwidth of cross dipoles, and the U-shaped metal reflecting cavity can further increase the impedance bandwidth (IBW) and axial ratio (AR) bandwidth of the antenna while enhancing HPBW and ARBW. To validate the feasibility of the design, the proposed antenna is fabricated and measured. The measured results show that the bandwidths of the antenna are 89.2% for -10 dB impedance and 82.7% for 3 dB AR. In addition, both HPBW and ARBW greater than 120° are achieved within a relative bandwidth of 63.1%.

1. INTRODUCTION

In recent years, the communication environment becomes increasingly more complex. Circularly polarized (CP) antennas with good interference immunity are widely used in many scenarios, such as wireless local area network, vehicle-mounted radar, and global positioning system. Additionally, wideband antennas, which facilitate multi-channel communication, have garnered extensive use in contemporary communication systems.

Nowadays, the reported wideband CP antennas with wide beamwidths are mostly realized by cross dipoles. In order to have a wider antenna impedance bandwidth (IBW), the reported methods can be divided into two categories: changing the dipole shape and loading parasitic elements. The reported dipoles include sector dipole [1], bow-tie dipole [2], stepped dipole [3], oval dipole [4], and barb dipole [5]. For loading parasitic elements, loading parasitic patches [6, 7], asymmetric cross loops [8], and a cavity reflector with four coupled rotated vertical metallic plates [9] have been proposed.

In addition to focusing on wideband, the circularly polarized antenna with wide axial-ratio beamwidth (ARBW) and wide half-power beamwidth (HPBW) is also a hot research direction. Loading metal reflection cavities has been proved to be an effective approach to improve ARBW and HPBW [10], while loading short-circuit metal plate can also be used to improve ARBW and HPBW [11, 12]. In addition, the cross-dipole antenna loaded with magnetoelectric dipoles obtains the ARBW of more than 165° [13]. By adding a notched-corner metal cavity around the antenna, the HPBW and ARBW are both greater than 110° in the operating band [14].

A broadband wide-beam CP antenna consisting of a fan-shaped crossed dipole and a U-shaped metallic reflecting cavity is proposed in the letter. The IBW and axial ratio (AR) bandwidths of the crossed dipole antenna are improved by modifying the rectangular electric dipole arm of the conventional crossed dipole antenna and introducing a fan-shaped patch. The loaded U-shaped metallic reflector cavity further increases the IBW and AR bandwidth of the antenna. In addition, the U-shaped metallic reflector cavity can be equated to four magnetic dipoles, whose radiation patterns are superimposed on those of the crossed dipoles, realizing the wide HPBW and ARBW of the antenna.

2. DESIGN OF ANTENNA

2.1. Antenna Structure

The configuration of the proposed antenna is displayed in Fig. 1. The antenna consists of a pair of cross dipoles and a U-shaped metal reflector cavity. Crossed dipoles are printed on the upper and lower surfaces of an F4B substrate ($\varepsilon_r = 2.55$, $\tan\delta = 0.002$). Four vertically placed U-shaped metal walls and the ground plane are constituted to a reflection cavity placed around the cross dipoles. It can be observed from Fig. 1(c) that the cross dipoles consisting of a pair of dipoles are perpendicular to each other. Each dipole consists of two dipole arms, and each dipole arm consists of a fan-shaped patch and a rectangular patch. The adjacent arms on the same layer are connected by a phase-shifting ring with $\lambda_g/4$ arc length to achieve a 90° phase difference, where λ_g is the guided wavelength at the center frequency. The inner conductor of the coaxial feed is routed through the substrate to connect with the dipole arm of the top layer, while the outer conductor is connected to the dipole arm of the bottom layer.

2.2. Antenna Mechanism

To illustrate the working mechanism of the proposed antenna, the evolution of the proposed antenna is shown in Fig. 2. In

* Corresponding author: Rui Deng (dengruinj@163.com).

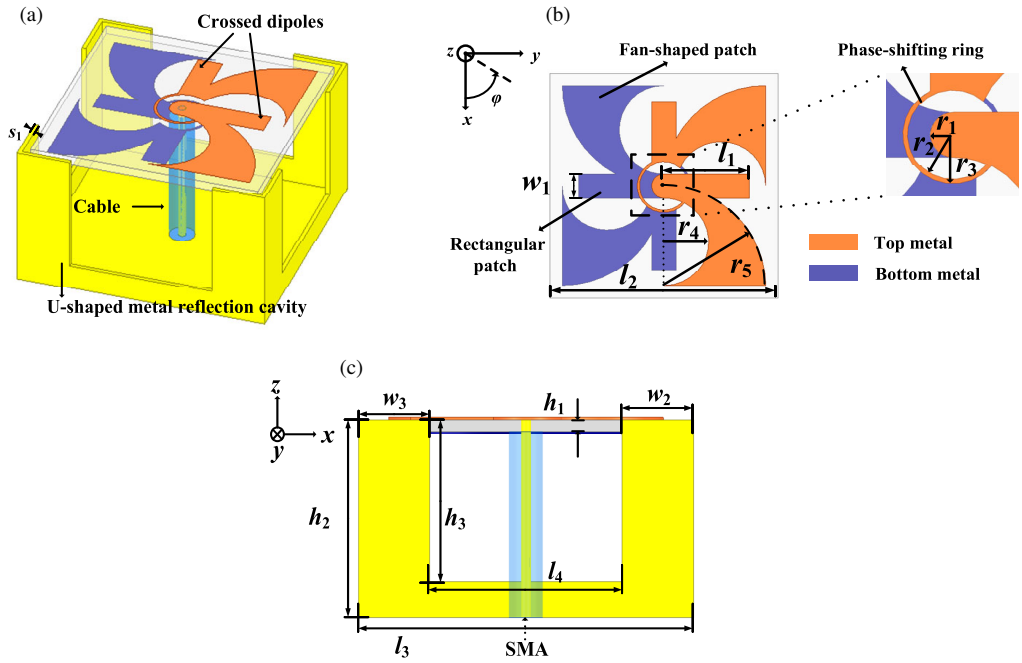

FIGURE 1. Geometry of the proposed antenna. (a) Stereoscopic view. (b) Top view. (c) Side view. $s_1 = 0.5\,\text{mm}$, $l_1 = 10.5\,\text{mm}$, $l_2 = 28\,\text{mm}$, $l_3 = 30.5\,\text{mm}$, $l_4 = 18.5\,\text{mm}$, $w_1 = 3.0\,\text{mm}$, $w_2 = 6\,\text{mm}$, $w_3 = 6\,\text{mm}$, $r_1 = 1.5\,\text{mm}$, $r_2 = 3.0\,\text{mm}$, $r_3 = 3.3\,\text{mm}$, $r_4 = 5.5\,\text{mm}$, $r_5 = 12.5\,\text{mm}$, $h_1 = 1.0\,\text{mm}$, $h_2 = 17.0\,\text{mm}$, $h_3 = 14.0\,\text{mm}$.

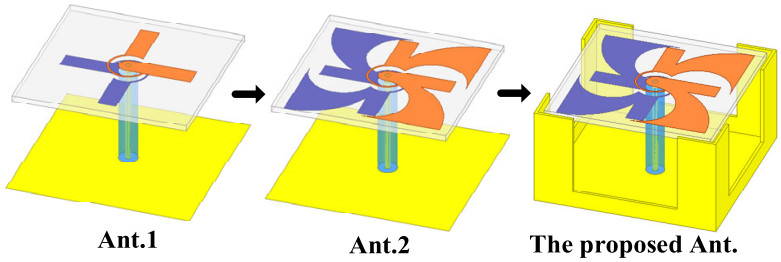

FIGURE 2. The evolution of the proposed antenna design.

Fig. 2, Ant.1 is a traditional crossed-dipole antenna with rectangular patch dipole arms, and the dipole arms are connected by a phase-shifting ring with $\lambda_g/4$ arc length. Ant.2 introduces four fan-shaped patches on the basis of Ant.1, and each fan-shaped patch is combined with an original rectangular patch to form a fan-shaped patch as a dipole arm of Ant.2. Subsequently, by incorporating four U-shaped metal walls around the dipole arms, Ant.2 is further evolved into the proposed antenna configuration. The metal walls are combined with the ground plane to form a metal reflection cavity.

For Ant.2, the lengths of the two dipoles satisfy the following two formulas:

$$l_1 \approx \frac{\lambda_{6.2\,\text{GHz}}}{4} \tag{1}$$

$$\pi r_4 \approx \frac{\lambda_{4.2\,\text{GHz}}}{4} \tag{2}$$

where $\lambda_{6.2\,\text{GHz}}$ and $\lambda_{4.2\,\text{GHz}}$ are the guided wavelengths of 6.2 GHz and 4.2 GHz, respectively. So, the rectangular patch and fan-shaped patch resonate around 6.2 GHz and 4.2 GHz, respectively. Therefore, when the fan-shaped patches are added, a resonance of 4.2 GHz is introduced to expand the operating bandwidth of the antenna to the low frequencies. The impedance change during the evolution of the antenna is shown by Fig. 4. It can be seen that at 4.0 GHz–6.0 GHz, $\text{Re}(Z_{11})$ is closer to 50 Ω, and $\text{Im}(Z_{11})$ is closer to 0 Ω for Ant.2 than for Ant.1. Therefore, Ant.2 is able to achieve a wider impedance bandwidth.

Beyond evaluating the impedance matching of the antenna, examining the operating modes of the crossed dipoles is also crucial for comprehending the strategy behind achieving a broader operating bandwidth with fan-shaped patch of Ant.2. The current distribution of Ant.2 using fan-shaped patches at 4.0 GHz and 6.0 GHz is shown in Fig. 5. It can be seen that when the antenna operates at 4.0 GHz, the current on the crossed dipole flows mainly periodically along the fan-shaped patch. And when the antenna operates at 6.0 GHz, the current on the cross dipole flows periodically along the rectangular patch in addition to the fan patch, so Ant.2 achieves an

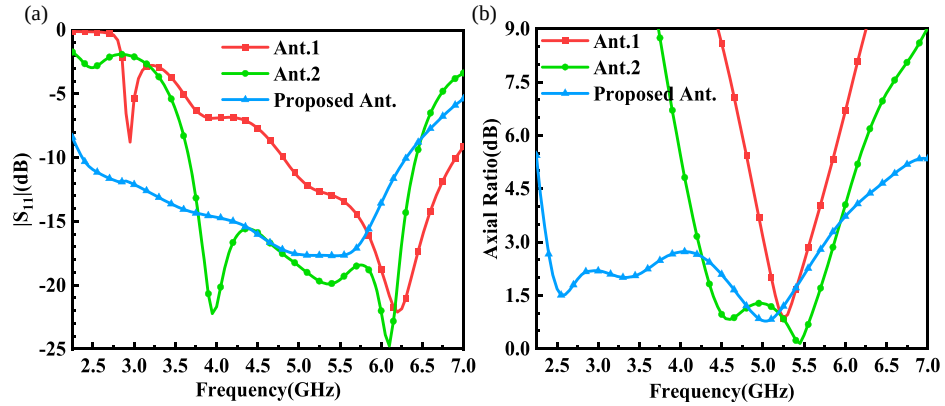

FIGURE 3. Simulated $|S_{11}|$ and ARs ($\varphi = 0^\circ$) for the evolution of the proposed antenna. (a) $|S_{11}|$. (b) ARs.

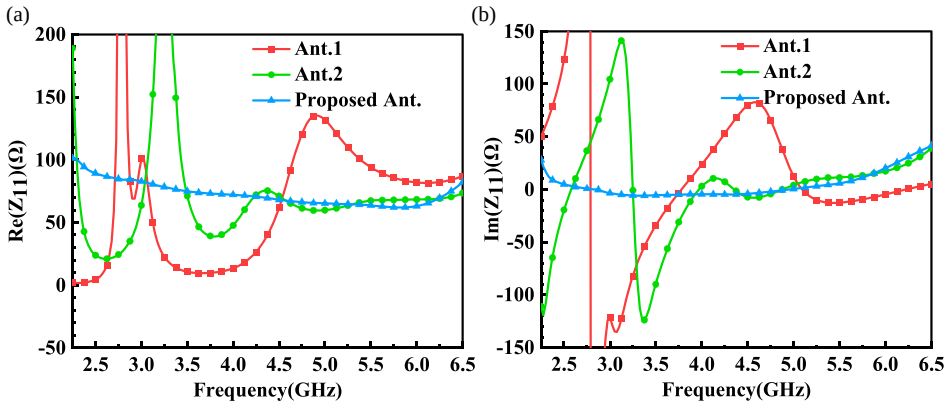

FIGURE 4. Simulated Z_{11} for the evolution of the proposed antenna. (a) Re(Z_{11}). (b) Im(Z_{11}).

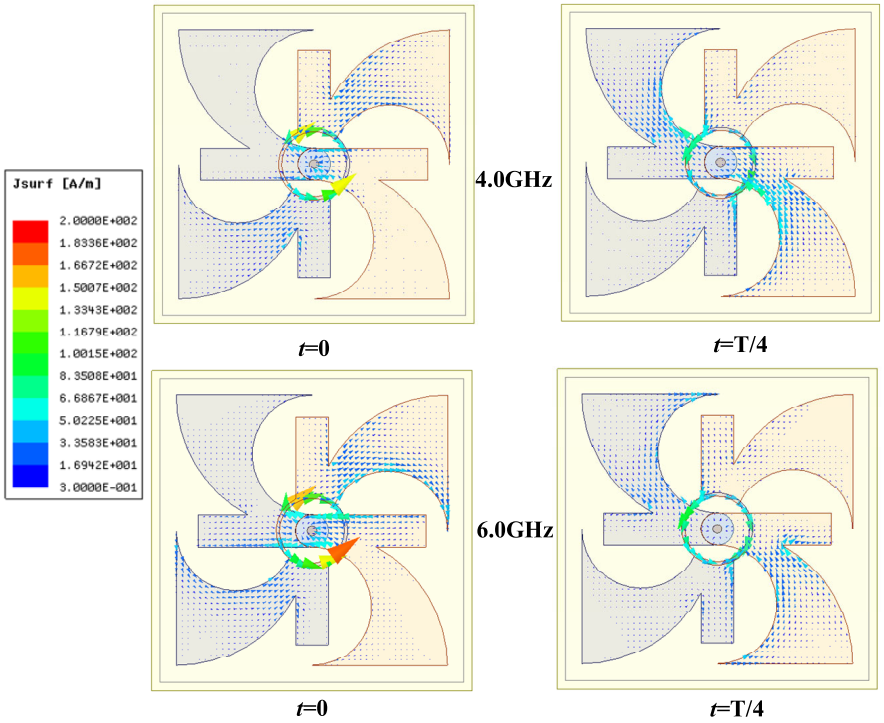

FIGURE 5. Simulated current distributions on the crossed fan-shaped dipoles of Ant.2 at 4.0 GHz and 6.0 GHz.

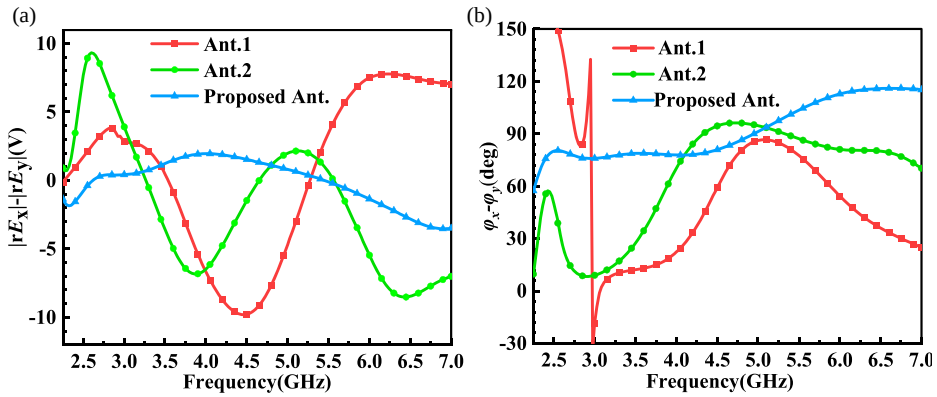

FIGURE 6. Plots of mutually perpendicular electric field amplitude differences and phase differences for the evolution of the proposed antenna. (a) Amplitude differences. (b) Phase differences.

increase in the bandwidth of the antenna by combining two patches with different resonant frequencies. Furthermore, upon combining the fan-shaped and rectangular patches, the current path deviates from flowing solely along either the rectangular or the fan-shaped patch. Instead, it traverses both patches, effectively elongating the current path. This extended path is responsible for the observed shift of the resonance point to a lower frequency upon the integration of the patches. Meanwhile, as shown in Fig. 6(b), the phase difference between the two electric fields E_x and E_y perpendicular to each other in the impedance bandwidth is improved after the addition of the curved patch on the dipole arm of Ant.2, which is closer to 90° than that of Ant.1, and thus the axial ratio bandwidth is improved. As shown in Fig. 3, the IBW of Ant.2 is improved from 35.8% (4.81–6.91 GHz) to 54.5% (3.67–6.42 GHz), and the AR bandwidth is improved from 10.5% (5.01–5.57 GHz) to 32.7% (4.22–5.87 GHz).

The proposed antenna loaded with the U-shaped metal reflection cavity further improves the IBW and AR bandwidth. This improvement is attributed to the close proximity between the U-shaped metal cavity and the edge of the fan-shaped patch of the crossed dipole, which induces a coupling effect. The coupling between the metal cavity and crossed dipole facilitates an improvement in impedance matching, consequently broadening the IBW of the antenna. From Fig. 4, it can be seen that the impedance matching of Ant.3 is greatly improved within 2.5 GHz–6.0 GHz. Compared with Ant.2, Re(Z_{11}) is closer to 50 Ω, and Im(Z_{11}) is closer to 0 Ω. The impedance change is also smoother, so that Ant.3 achieves a wider impedance bandwidth. While the Re(Z_{11}) of the proposed antenna near 4 GHz becomes about 70 Ω from close to 50 Ω in Ant.2, the original resonance point near 4 GHz becomes no longer obvious, so the smoother impedance variation in the low frequency band of the proposed antenna obtains a wider impedance bandwidth at the same time, which results in a resonance point that is not as clear as that of Ant.2.

Meanwhile, as shown in Fig. 6, it is due to the loading of the U-shaped metal cavity that not only makes the amplitude difference between the two electric fields E_x and E_y perpendicular to each other in the entire impedance bandwidth close to 0, but also improves the phase difference of the electric field between 2.5 GHz and 4.0 GHz to be closer to 90° compared to Ant.2, and thus the axial ratio of the proposed antenna in the lower frequency band is improved. It can be seen that the IBW of the proposed antenna is improved to 90.7% (2.37–6.31 GHz), and the AR bandwidth is improved to 83.3% (2.37–5.76 GHz). In addition, as shown in Fig. 7, the loading of U-shaped metal reflection cavity makes the beamwidth of the proposed antenna significantly enhanced, and the average HPBW of the antenna in the IBW is improved to 114° from 74° of Ant.2, and the 3-dB ARBW is also significantly improved. In addition, the average radiation efficiency of the antenna is 95.51% over the operating bandwidth of the proposed antenna.

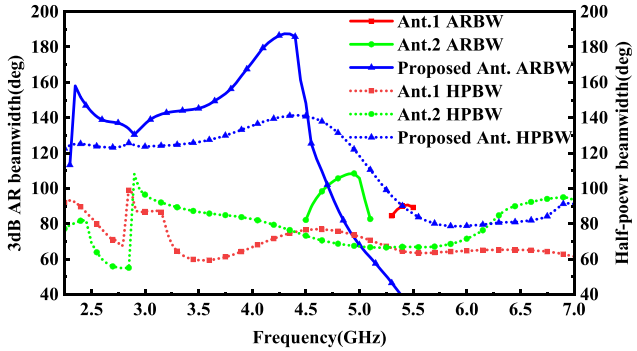

FIGURE 7. Simulated HPBW and 3-dB ARBW for the evolution of the proposed antenna.

2.3. Parameters Studies

The proposed antenna has a simple structure, and this section delves into several pivotal parameters to delineate its performance comprehensively. In this study, all the simulations are performed by Ansoft High Frequency Structure Simulator based on the finite element method. All the parameters stay the same unless stated.

Firstly, the effects of the variation of the crossed dipole rectangular patch length l_1 and the fan-shaped patch radius r_5 on the proposed antenna are analyzed. As shown in Fig. 8, the impedance bandwidth of the antenna is almost unchanged when l_1 is gradually increased from 10 mm to 11.5 mm, and it is worth noting that the low-frequency $|S_{11}|$ of the antenna slightly

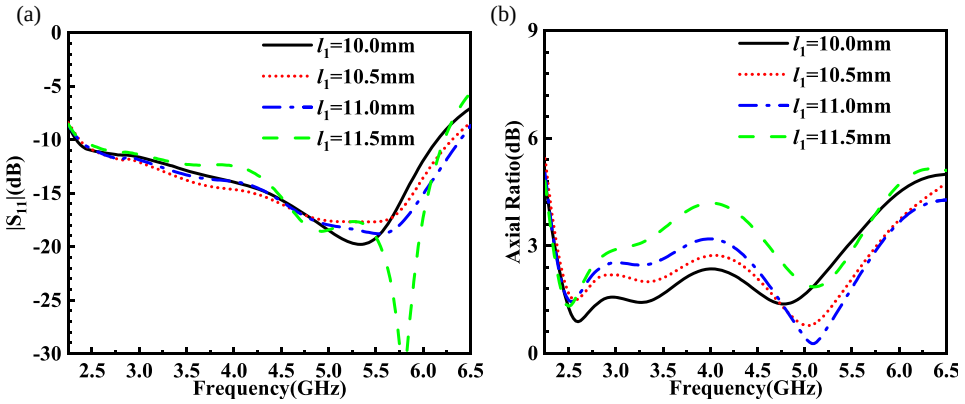

FIGURE 8. Effects of various l_1 on (a) $|S_{11}|$ and (b) AR.

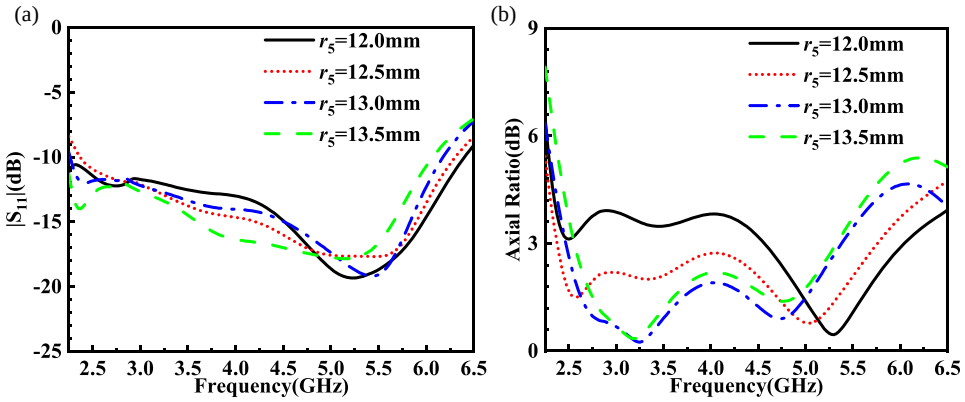

FIGURE 9. Effects of various r_5 on (a) $|S_{11}|$ and (b) AR.

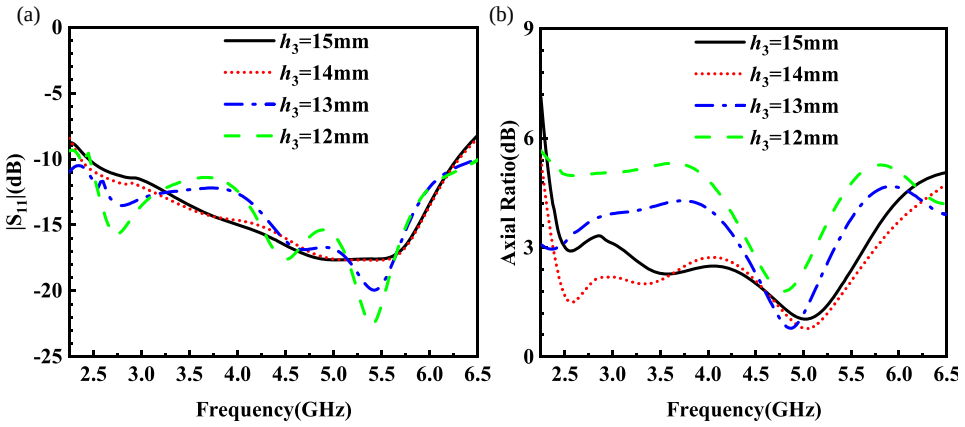

FIGURE 10. Effects of various h_3 on (a) $|S_{11}|$ and (b) AR.

deteriorates, and the high-frequency resonance point becomes clearer when $l_1 = 11.5$ mm. The increase of l_1 causes the deterioration of the AR of the antenna at low frequencies. When $l_1 = 10.5$ mm, the antenna achieves the widest AR bandwidth at this time, so considering the operating bandwidth of the antenna, the final value of l_1 is set to 10.5 mm. The effect of the change of r_5 on the proposed antenna is shown in Fig. 9, and the resonance point of the antenna is shifted to the low frequency with the increase of r_5. Similar to l_1, the variation of r_5 has less effect on the impedance bandwidth of the antenna. As r_5 increases, the AR of the antenna becomes smaller in the low frequency band, but the AR in the high frequency band gets deteriorated. When $r_5 = 12.5$ mm, the antenna achieves the widest axial ratio bandwidth, so the final value of r_5 is 12.5 mm.

Next, the effect of the variation of the U-shaped metal cavity parameters on the proposed antenna is analyzed. Fig. 10 shows the variation of $|S_{11}|$ and AR as h_3 decreases. From Fig. 10(a), it can be seen that the decrease of h_3 makes the

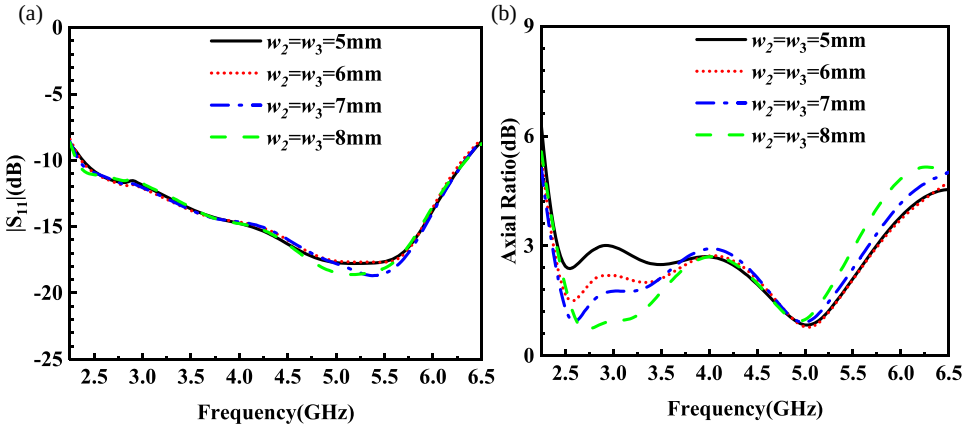

FIGURE 11. Effects of various w_2 and w_3 on (a) $|S_{11}|$ and (b) AR.

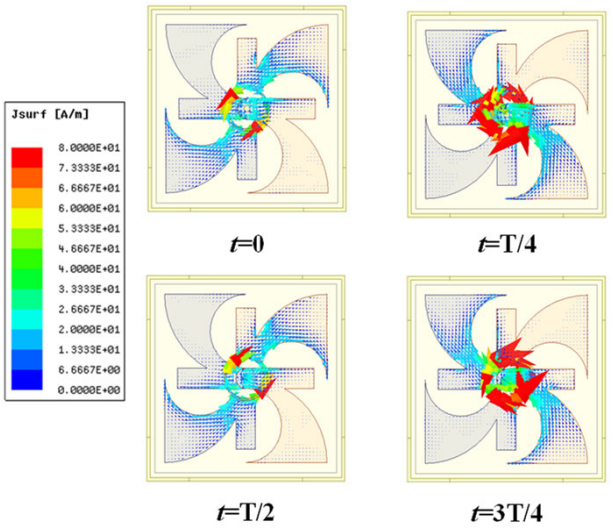

FIGURE 12. Simulated current distributions on the crossed dipoles at 3.6 GHz.

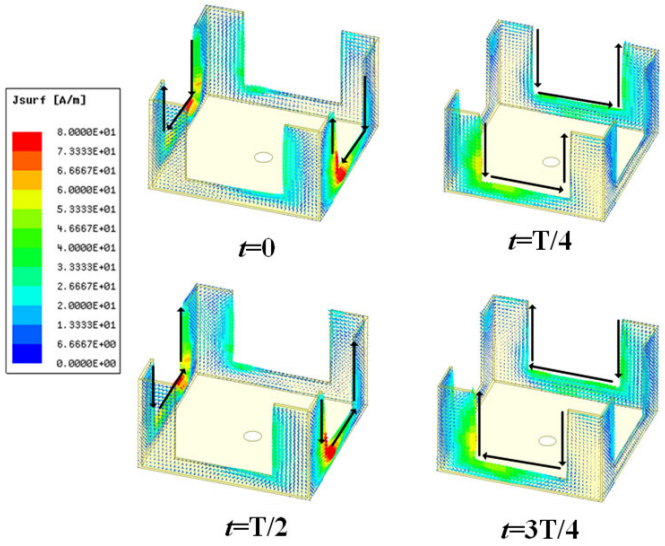

FIGURE 13. Simulated current distributions on the U-shaped metal reflector cavity at 3.6 GHz.

resonance point of the antenna more obvious, and $|S_{11}|$ of the antenna is smoother when $h_3 = 15$ mm and $h_3 = 14$ mm. At $h_3 = 13$ mm and $h_3 = 12$ mm, three resonance points of the antenna can be clearly seen, which are 2.75 GHz, 4.5 GHz, and 5.4 GHz, respectively, whereas it can be seen from Fig. 10(b) that the effect of the change of h_3 on the AR bandwidth is significant, and the antenna has a wider 3-dB AR bandwidth only when $h_3 = 14$ mm. When $h_3 = 12$ mm and $h_3 = 13$ mm, the AR bandwidth becomes worse in the whole frequency band, while when $h_3 = 15$ mm, the AR bandwidth becomes worse in the lower frequency band.

Then, the widths of the U-shaped metal cavity w_2 and w_3 are investigated. Fig. 11 shows the effect of gradual increase of w_2 and w_3 on the antenna $|S_{11}|$ and AR. From Fig. 11(a), it can be seen that the increase of w_2 and w_3 has basically no effect on antenna $|S_{11}|$. From Fig. 11(b), it can be seen that the axial ratio of the antenna at the low frequency becomes gradually lower as w_2 and w_3 increase from 5 mm to 8 mm, but at the same time, the AR of the antenna at the center frequency point as well as at the high frequency deteriorates slightly. In order to ensure the continuity of the axial ratio bandwidth and to achieve the widest axial ratio bandwidth, the values of w_2 and w_3 are chosen to be 6 mm, when the axial ratio at the center frequency is less than 3 dB, and the antenna achieves the widest axial ratio bandwidth.

2.4. Wide Beam Principle Analysis of the Antenna

The working principle of the proposed antenna can be further analyzed. Fig. 12 and Fig. 13 show the current distributions of the crossed dipole and the U-shaped metal reflection cavity with different phases in one cycle. By observing the simulated different currents distributions on the crossed dipole in one cycle, it can be observed that the current distributions with a phase difference of 90° are perpendicular to each other, and the amplitudes of the currents are almost equal, so the crossed dipole has a good CP characteristic. On the U-shaped metal reflection cavity, the current distributions with a phase difference of 90° are also perpendicular to each other, and the amplitudes of the

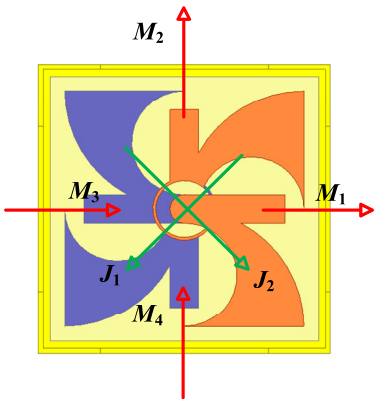

FIGURE 14. Electric and magnetic dipole combinations for the proposed antenna equivalent.

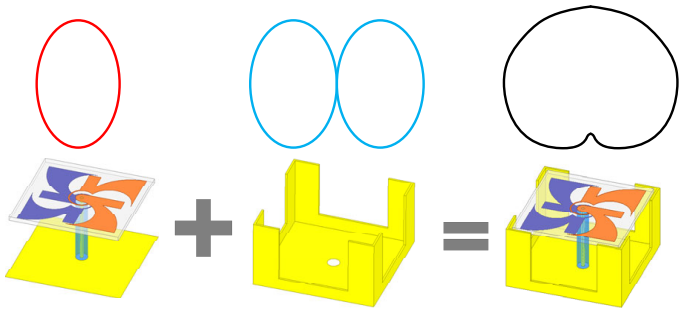

FIGURE 15. Principle of beam superposition.

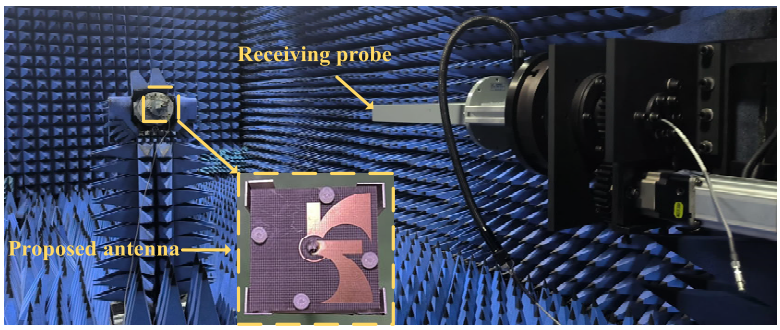

FIGURE 16. Photograph of the proposed antenna and far-field measurement environment.

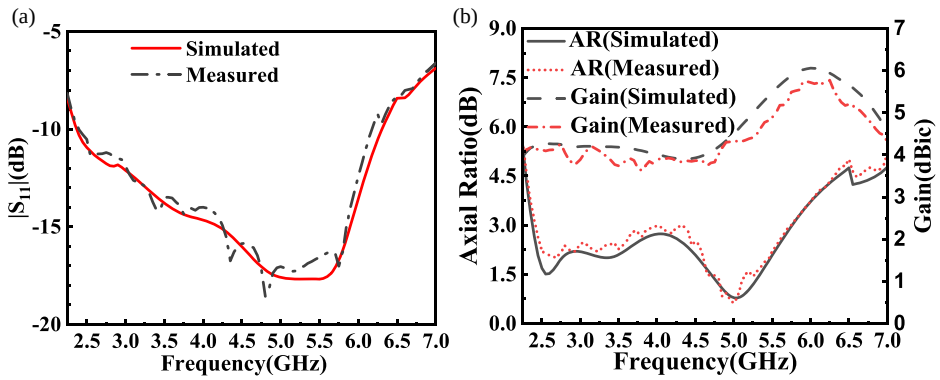

FIGURE 17. The $|S_{11}|$, gains and ARs of the antenna. (a) $|S_{11}|$. (b) Boresight gains and ARs.

currents are almost equal, so the crossed dipole antenna maintains good CP characteristics after loading the U-shaped metal reflection cavity. Therefore, in Fig. 3 and Fig. 7, after loading the U-shaped metal reflection cavity the antenna exhibits a wider AR bandwidth and can maintain a wide ARBW over a wider bandwidth.

The reason that the proposed antenna is able to accomplish wide HPBW within a wideband can be explained by the beam superposition principle of electric and magnetic dipoles. Any one wall of the U-shaped metal reflection cavity is chosen as can be seen in Fig. 13. The simulated current flows in a U-shape along the metal wall in one cycle, which can be regarded as a toroidal current, and thus equivalent to a magnetic dipole, so that the four metal walls of the U-shape metal reflection cavity can be equivalent to four magnetic dipoles. Therefore, the proposed antenna can be equated to two electric dipoles and four magnetic dipoles as shown in Fig. 14. It is well known that the E-plane and H-plane radiation patterns of an electric dipole are figure-8 and O shaped, respectively, while the opposite is true for a magnetic dipole. The beam of the proposed antenna can be regarded as the beams of the crossed dipoles superimposed on the beams of the U-shaped metal cavity, and the principle of beam superposition is shown in Fig. 15.

TABLE 1. Comparison of the proposed antenna with previously reported wide-beam circularly polarized antennas.

Ref.	Impedance Bandwidth	AR Bandwidth	Overlapping Bandwidth	Maximum ARBW (Bandwidth)	Maximum HPBW (Bandwidth)	Gain (dBic)
[10]	46%	47.2%	41.3%	-	120°(> 100 : 30.1%)	5.8
[11]	92.6%	71.8%	71.8%	−(> 120° : 70.3%)	−(> 100° : 62.8%)	3.9
[12]	78.3%	63.4%	63.4%	196°(> 120° : 50.7%)	154°(> 110° : 61.1%)	4.7
[14]	16.5%	1.9%	1.9%	165°	143°	2.6
[15]	32.5%	7.5%	7.5%	161°(> 120° : 34.4%)	129°(> 110° : 34.4%)	3.5
Prop	89.2%	82.7%	**82.7%**	185°(> 120° : 63.1%)	142°(**> 120° : 71.1%**)	5.7

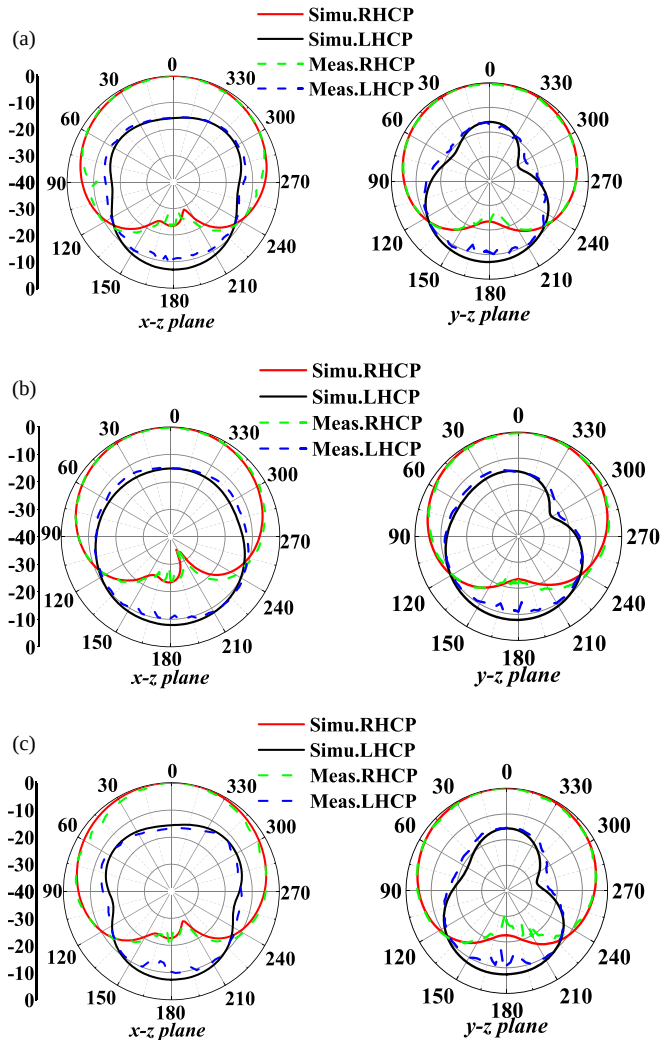

FIGURE 18. The radiation patterns of the proposed antenna. (a) 2.5 GHz. (b) 4 GHz. (c) 5.5 GHz.

3. SIMULATED AND MEASURED RESULTS

In order to verify the feasibility of the proposed antenna, a prototype as shown in Fig. 1 is fabricated. The crossed-dipole is printed on an F4B substrate with $h_1 = 1$ mm and $\varepsilon_r = 2.55$. The ground plane and U-shaped metal wall are made of metallic aluminum, and the fabricated antenna and measuring environment are displayed in Fig. 16. Fig. 17(a) shows the simulated and measured $|S_{11}|$. The measured IBW of the antenna is obtained as 89.2% (2.4–6.27 GHz). The boresight gains and ARs are displayed in Fig. 17(b). The antenna is achieved a 3 dB AR bandwidth of 82.7% (2.35–5.75 GHz), and the average gain over the IBW is 4.3 dBic. The antenna gain is increased from 4.0 to 5.8 dBic in the frequency ranged from 4.5 to 6.0 GHz, because the designed antenna has a decrease in HPBW at higher frequency in Fig. 7.

The simulated and measured radiation patterns of the proposed antenna at different frequencies are displayed in Fig. 18. As it shows, the antenna has stable broad beam radiation patterns at 2.5 GHz, 4 GHz, and 5.5 GHz as expected. It can be observed that along the z-axis direction, the right-hand circular polarization (RHCP) of the antenna is more than 15 dB larger than the left-hand circular polarization (LHCP) gain. So, it can be obtained that the antenna has good RHCP performance. There are some differences between the measured and simulated results, which are caused by the errors in the manufacturing and measurement processes of the antenna.

To further demonstrate the superior performance of the proposed antenna, the proposed antenna and the previously reported wide-beam CP antennas are compared in Table 1. It can be seen that the proposed antenna has wider operating bandwidth, good ARBW bandwidth, and excellent HPBW bandwidth, while maintaining good gain and normal back lobe. Therefore, the overall performance of the proposed antenna is superior to the previously reported wide bandwidth wide beam CP antennas.

4. CONCLUSIONS

A fan-shaped crossed dipole CP antenna loaded with a U-shaped metallic reflector cavity is investigated in the paper. The fan-shaped patch can increase the IBW and optimize the axial ratio of the antenna, and the loaded U-shaped metal reflection cavity can further increase the IBW and 3-dB AR bandwidth of the antenna. Meanwhile, loading the U-shaped metal reflection cavity improves the HPBW and ARBW of the antenna. A prototype is fabricated, and measurements are performed to verify the design. The proposed antenna achieves 89.2% IBW with 82.7% 3 dB AR bandwidth and can achieve greater than 120° HPBW and ARBW over 63.1% relative bandwidth.

ACKNOWLEDGEMENT

This work was supported by the Scientific and Technological Research Program of Chongqing Municipal Education Commission (KJQN202300611), Chongqing Postgraduate Research and Innovation Project (CYS22445).

REFERENCES

[1] Feng, Y., J. Li, B. Cao, J. Liu, G. Yang, and D.-J. Wei, "Cavity-backed broadband circularly polarized cross-dipole antenna," *IEEE Antennas and Wireless Propagation Letters*, Vol. 18, No. 12, 2681–2685, Dec. 2019.

[2] Mak, K. M. and K. M. Luk, "A circularly polarized antenna with wide axial ratio beamwidth," *IEEE Transactions on Antennas and Propagation*, Vol. 57, No. 10, 3309–3312, Oct. 2009.

[3] Yang, W., Y. Pan, S. Zheng, and P. Hu, "A low-profile wideband circularly polarized crossed-dipole antenna," *IEEE Antennas and Wireless Propagation Letters*, Vol. 16, 2126–2129, May 2017.

[4] He, W., Y. He, Y. Li, S.-W. Wong, and L. Zhu, "A compact ultrawideband circularly polarized antenna array with shared partial patches," *IEEE Antennas and Wireless Propagation Letters*, Vol. 20, No. 12, 2280–2284, Dec. 2021.

[5] Tran, H. H. and I. Park, "A dual-wideband circularly polarized antenna using an artificial magnetic conductor," *IEEE Antennas and Wireless Propagation Letters*, Vol. 15, 950–953, Oct. 2015.

[6] Zhao, Z., Y. Li, M. Xue, L. Wang, Z. Tang, and Y. Yin, "Design of wideband circularly polarized crossed-dipole antenna using parasitic modified patches," *IEEE Access*, Vol. 7, 75 227–75 234, Jun. 2019.

[7] Yang, W.-J., Y.-M. Pan, and S.-Y. Zheng, "A compact broadband circularly polarized crossed-dipole antenna with a very low profile," *IEEE Antennas and Wireless Propagation Letters*, Vol. 18, No. 10, 2130–2134, Oct. 2019.

[8] Feng, G., L. Chen, X. Xue, and X. Shi, "Broadband circularly polarized crossed-dipole antenna with a single asymmetrical cross-loop," *IEEE Antennas and Wireless Propagation Letters*, Vol. 16, 3184–3187, Oct. 2017.

[9] Fan, J., J. Lin, J. Cai, and F. Qin, "Ultra-wideband circularly polarized cavity-backed crossed-dipole antenna," *Scientific Reports*, Vol. 12, No. 1, 4569, Mar. 2022.

[10] Chen, L., T.-L. Zhang, C. Wang, and X.-W. Shi, "Wideband circularly polarized microstrip antenna with wide beamwidth," *IEEE Antennas and Wireless Propagation Letters*, Vol. 13, 1577–1580, Jul. 2014.

[11] Li, G. and F.-S. Zhang, "A compact broadband and wide beam circularly polarized antenna with shorted vertical plates," *IEEE Access*, Vol. 7, 90 916–90 921, Jul. 2019.

[12] Yang, W. J., Y. M. Pan, and S. Y. Zheng, "A low-profile wideband circularly polarized crossed-dipole antenna with wide axial-ratio and gain beamwidths," *IEEE Transactions on Antennas and Propagation*, Vol. 66, No. 7, 3346–3353, Jul. 2018.

[13] Ta, S. X. and I. Park, "Crossed dipole loaded with magneto-electric dipole for wideband and wide-beam circularly polarized radiation," *IEEE Antennas and Wireless Propagation Letters*, Vol. 14, 358–361, Oct. 2014.

[14] Zhang, T., H. Liu, S.-J. Fang, and Z. Wang, "Single-fed wide-beamwidth circularly polarized antenna using reflector-loaded bent dielectric resonator," *Progress In Electromagnetics Research Letters*, Vol. 109, 65–73, 2023.

[15] Li, C., F.-S. Zhang, F. Zhang, and K. Yang, "A wideband circularly polarized antenna with wide beamwidth for GNSS applications," *Progress In Electromagnetics Research C*, Vol. 84, 189–200, 2018.